PHYSICAL REVIEW B **88**, 161304(R) (2013)

Nonequilibrium dynamics in an optical transition from a neutral quantum dot to a correlated many-body state

F. Haupt,[1,*] S. Smolka,[1] M. Hanl,[2] W. Wüster,[1] J. Miguel-Sanchez,[1] A. Weichselbaum,[2] J. von Delft,[2] and A. Imamoglu[1]

[1]*Institute of Quantum Electronics, ETH Zürich, CH-8093, Zürich, Switzerland*

[2]*Arnold Sommerfeld Center for Theoretical Physics, Ludwig-Maximilians-Universität München, D-80333 München, Germany*

(Received 4 April 2013; revised manuscript received 21 August 2013; published 28 October 2013)

We investigate the effect of many-body interactions on the optical absorption spectrum of a charge-tunable quantum dot coupled to a degenerate electron gas. A constructive Fano interference between an indirect path, associated with an intradot exciton generation followed by tunneling, and a direct path, associated with the ionization of a valence-band quantum dot electron, ensures the visibility of the ensuing Fermi-edge singularity despite weak absorption strength. We find good agreement between experiment and renormalization group theory, but only when we generalize the Anderson impurity model to include a static hole and a dynamic dot-electron scattering potential. The latter highlights the fact that an optically active dot acts as a tunable quantum impurity, enabling the investigation of a new dynamic regime of Fermi-edge physics.

DOI: 10.1103/PhysRevB.88.161304 PACS number(s): 78.67.Hc, 73.20.−r, 73.21.La, 78.30.Fs

When a fermionic reservoir (FR) experiences a dynamically changing local perturbation, all its eigenstates are modified in response; the resulting Anderson's orthogonality catastrophe[1] plays a central role in the physics of quantum impurity systems. Along with the Kondo effect,[2–6] the most extensively studied quantum impurity problem is the Fermi-edge singularity (FES):[7–10] an optical absorption event induces a local quantum quench, causing dynamical changes in reservoir states that lead to power-law tails in the absorption line shape. This has been observed, for example, in the context of x-ray absorption in metals,[11–13] where a large ensemble of deep-level states were ionized upon absorption and the resulting collective modification of the absorption line shape was measured. A related many-body effect has also been investigated in semiconductor structures incorporating a degenerate electron gas:[14–16] In these studies, the modification of the absorption line shape is due to a rearrangement of the conduction-band electrons after the creation of an electrostatic potential by photoexcited quasimobile valence-band holes.

In this Rapid Communication, we report the observation of a FES due to a single localized hole in a charge-tunable quantum dot (QD) and a tunnel-coupled FR. In our experiments, the ionization of a QD valence-band electron takes place via two competing paths: (1) excitation of a QD neutral exciton followed by ionization due to tunneling of the conduction-band electron into the FR, and (2) a direct transition from a QD valence band to an electronic state above the Fermi level of the FR. While in the classic x-ray absorption experiments only the latter process is relevant, in our experiments both contribute to single-photon absorption. Since both paths lead to final states of identical structure, involving a single-hole charged QD and a FR whose eigenstates are modified by the QD scattering potential, we observe a Fano interference.[17] Thanks to the constructive nature of this interference we can observe the signature of the FES despite the small transition probability associated with path (2). The presence of path (1) is also responsible for the dynamical local screening of the hole potential. Tuning the energy of the QD electron level with respect to the Fermi energy allows us to change the residual electron charge on the QD continuously, thereby varying the strength of the effective hole scattering potential. While in earlier optical experiments[18–23] a FES was observed by creating an undefined number of positive hole charges in the FR, we generate the electrostatic scattering potential by a single localized hole on a QD, defining a spatially well-isolated impurity.[10,24–26] From resonant absorption measurements we can determine the dynamics of the potential scattering as well as the Fano parameters of the correlated many-body state.

Setup. The quantum impurity system under study,[27] consists of a single shallow self-assembled InAs QD with the neutral exciton resonance at $\lambda \approx 891.25$ nm, tunnel coupled to a 40-nm n^{++} back gate and an $In_{0.08}Ga_{0.92}As$ 7 nm quantum well that is 9 nm below the QDs. The system is embedded in a Schottky diode structure, in order to allow continuous tuning between different charging regimes.[28,29] Resonant laser spectroscopy measurements are carried out with a fiber-based confocal microscope setup (numerical aperture NA = 0.55) that is embedded in a dilution refrigerator. Figure 1(a) shows low-temperature differential transmission measurements of the energy plateaus of the neutral QD exciton (X^0) and single-negatively charged QD exciton (X^-) as a function of applied gate voltage. At the edges of the charging plateaus we observe an energy renormalization towards lower (higher) energies for the neutral (charged) QD transition, which is a hallmark of a strong tunnel coupling to a nearby FR.[5,30]

Measured absorption spectra. To probe the role of many-body interactions, we carried out high-resolution laser scans for various representative gate voltages in the X^0 plateau [Fig. 1(b)]. Tuning the gate voltage to lower values allows us to increase the energy of the QD electron levels with respect to the Fermi energy. The absorption line shapes [$A(\Delta E)$] obtained for various gate voltages thus show the gradual evolution of the system from a regime where the final state is an excited QD state [Fig. 1(d)] to the one in which it can be described by an optically excited electron in the FR and a hole trapped in the QD [Fig. 1(i)]. We emphasize that for our sample the latter state has a dipole moment that is approximately a factor of 2 larger than the dipole moment of the X^0.

When the QD X^0 state approaches the Fermi energy, the absorption line shape consists of two peaks: the

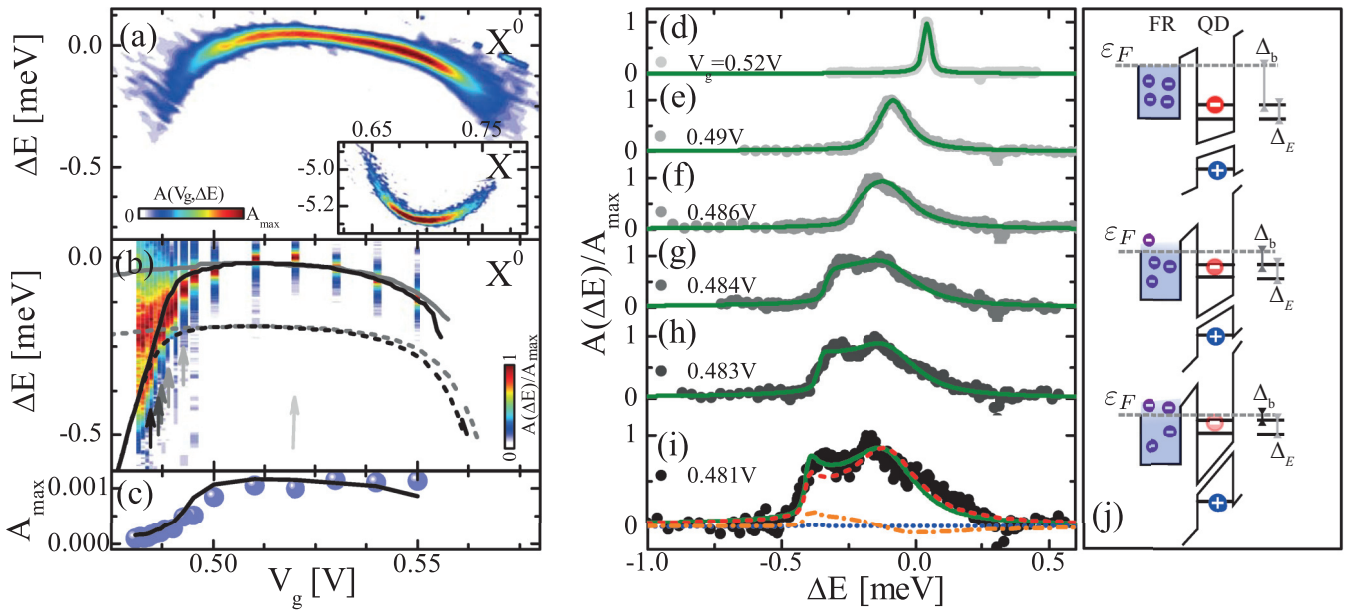

FIG. 1. (Color online) (a) Differential transmission measurements of the X^0 and the X^- (inset) QD charging states, after subtracting the dc Stark shift (Ref. 27). $\Delta E = E - E_0$ incorporates the peak absorption energy $E_0 = 1.3913$ eV at $V_g = 0.52$ V. (b) High-resolution laser absorption scans (color scale) at selected gate voltages. Solid lines show fits of the calculated lowest-energy peak position, $\Delta E_{\rm peak}$, either without the scattering potential ($H_{\rm S}^a = 0$, solid gray), or including it ($H_{\rm S}^a \neq 0$, solid black). Dashed lines show the ground state energy difference, $\hbar\omega_{\rm th}$, between the initial and final states of the absorption process, calculated for $H_{\rm S}^a = 0$ (dashed gray) or $H_{\rm S}^a \neq 0$ (dashed black). The difference $\Delta E_{\rm peak} - \hbar\omega_{\rm th}$ is on the order of the dark-bright splitting Δ_E in the plateau center. (c) Comparison of the measured (dots) and calculated (curve) maximum absorption amplitudes (the latter scaled vertically by an overall fixed oscillator strength), shown as a function of gate voltage. (d)–(i) Measured absorption line shapes of the transition from a neutral exciton to a correlated many-body state (normalized by the experimental peak height $A_{\rm max}$) at gate voltages indicated by corresponding color-coded arrows in (b). The green curves display calculated results, scaled vertically and shifted horizontally to minimize the χ^2 value of each fit (Ref. 27). The absorption components of the direct (red dashed), indirect (blue dotted), and interference (orange dash-dotted) terms are exemplarily depicted in (i). Since the tail of the X^0 state spectrally overlaps with the X^+ state, we can excite the latter, which shows up as a dip in the absorption line shapes for red detunings. (j) Schematic of the renormalized transition energies of the bright $\varepsilon_F - \Delta_{\rm b}$ and dark $\varepsilon_F - \Delta_{\rm b} - \Delta_E$ electron levels with respect to the Fermi energy $\varepsilon_{\rm F}$ directly after the single-photon absorption event. $\Delta_{\rm b}$ indicates the energy difference between the Fermi energy and the bright state, corresponding to the line shape shown in (d) (top), in (f) (middle), and in (i) (bottom).

higher-energy peak corresponding to the X^0 transition that is tunnel broadened, and a second, lower-energy peak associated with the onset of absorption from the QD valence band directly into the FR [Fig. 1(i)]. As we argue below, this second peak carries the signatures of a many-body resonance and reveals its nonequilibrium dynamics that is the focus of our work.

Model. In order to understand the various features of the absorption line shapes depicted in Figs. 1(d)–1(i), we generalize the excitonic Anderson model (EAM), previously used to describe the optical signatures of the Kondo effect,[5,6] by including a dynamic scattering potential:

$$H_A^a = H_{\rm QD}^a + H_{\rm FR} + H_{\rm S}^a, \tag{1}$$

$$H_{\rm QD}^a = \sum_\sigma \varepsilon_\sigma^a(V_g)\,\hat{n}_\sigma + U_{\rm ee}\,\hat{n}_\uparrow\hat{n}_\downarrow + \delta_{a,f}\,\varepsilon_h(V_g), \tag{2}$$

$$H_{\rm FR} = \sum_{k\sigma}[\varepsilon_{k\sigma}\,\hat{c}_{k\sigma}^\dagger\hat{c}_{k\sigma} + \sqrt{\Gamma/(\pi\,\rho)}\,(\hat{e}_\sigma^\dagger\hat{c}_{k\sigma} + \text{H.c.})], \tag{3}$$

$$H_{\rm S}^a = \left[G_{\rm ee}\left(\sum_\sigma \hat{n}_\sigma\right) - G_{\rm eh}\,\delta_{a,f}\right]\sum_{\sigma'}\left(\hat{\Psi}_{\sigma'}^\dagger\hat{\Psi}_{\sigma'} - \frac{1}{2}\right). \tag{4}$$

Here, $a = i, f$ differentiates between the initial (i) Hamiltonian before absorption [Fig. 2(a)], and the final (f) Hamiltonian [Fig. 2(d)] after creation of an exciton. In the QD Hamiltonian $H_{\rm QD}^a$ the electron occupancy is denoted as $\hat{n}_{\sigma=\uparrow,\downarrow} = \hat{e}_\sigma^\dagger\hat{e}_\sigma$. We assume a static hole spin and denote the bright state by $|\uparrow\Downarrow\rangle$ and the dark state by $|\downarrow\Downarrow\rangle$.[31] The bare energy of the electronic level, measured with respect to the Fermi energy ($\varepsilon_{\rm F} = 0$), is given by $\varepsilon_\sigma^a(V_g) = \varepsilon_0(V_g) - \delta_{a,f}(U_{\rm eh} + \delta_{\sigma,\downarrow}\Delta_E)$, where $\delta_{a,f}$ is the Kronecker delta and Δ_E is the dark-bright splitting. Both the conduction-band electron [$\varepsilon_0(V_g) = \varepsilon_0 - |e|V_g l$] and valence-band hole [$\varepsilon_h(V_g) = -\varepsilon_{h,0} + |e|V_g l$] state energies shift linearly with the gate voltage, l being the voltage-to-energy conversion factor (lever arm). The energy of the optically excited QD states is lowered by the Coulomb attraction $U_{\rm eh}$ and lifted by the on-site Coulomb repulsion $U_{\rm ee}$. $H_{\rm FR}$ describes the FR as a noninteracting conduction band with bandwidth W, symmetric around $\varepsilon_{\rm F}$, and constant density of states $\rho = 1/W$ per spin, tunnel coupled to the QD, where $\hat{\Psi}_\sigma = \sum_k \hat{c}_{k\sigma}$ annihilates a FR electron at the QD position and Γ is the tunneling rate. Finally, the dynamic scattering potential $H_{\rm S}^a$, which becomes important in the crossover between the local moment and free orbital regimes ($\varepsilon_\sigma^f \gtrsim 0$),[25] describes the contact Coulomb attraction, $G_{\rm eh}$, and repulsion, $G_{\rm ee}$, between FR electrons and the QD hole or QD electrons, respectively, as depicted in Fig. 2(d). Note that the effective scattering strength depends on the QD occupation and thus on the screened QD hole charge.

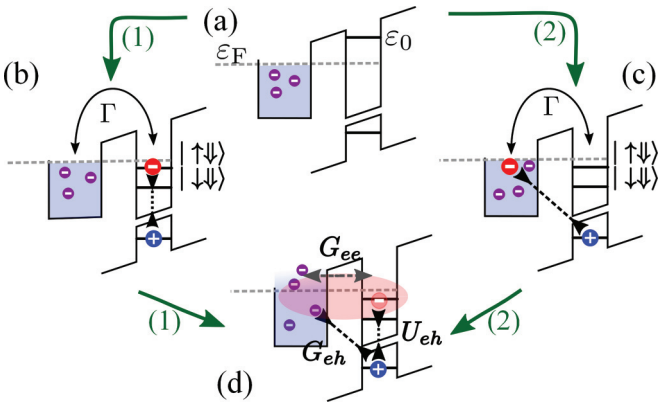

FIG. 2. (Color online) Scheme of the quantum impurity system consisting of a single QD and a nearby FR. (a) Initial quantum state where the QD with energy ε_0 above the Fermi energy ε_F is empty and the FR is unperturbed. The absorption of a single photon leads either (b) to a bound exciton on the QD or (c) to an indirect exciton. (d) The final state as $t \to \infty$ involves many-body correlations (red) between the FR and the QD. The black dashed and dotted lines depict the scattering potential between QD and FR, or the intradot Coulomb attraction, respectively.

Fano interference. Starting from a neutral QD [Fig. 2(a)], a photon absorption event can either create a QD exciton, involving $\hat{e}^\dagger_\uparrow$ [Fig. 2(b)], or an indirect exciton, involving $\hat{\Psi}^\dagger_\uparrow$ [Fig. 2(c)]. Both of these intermediate states evolve into a common final state [Fig. 2(d)], where the QD hole scattering potential modifies the eigenstates of the FR due to the partial ionization of the QD and scattering of the FR electrons by the unscreened charge. The resulting absorption spectrum is given by

$$A(\nu) = \alpha^2 A_{\rm QD}(\nu) + (1-\alpha)^2 A_{\rm FR}(\nu) + 2\alpha(1-\alpha)\cos(\phi) A_{\rm I}(\nu), \quad (5)$$

with α being the branching ratio between the two optical paths and a Fano phase $\phi = 0$ or $\phi = \pi$.[27] $\nu = \omega - \omega_{\rm th}$ describes the detuning between the laser frequency ω and the ground state energy difference, $\omega_{\rm th} = (E^{\rm f}_{\rm G} - E^{\rm i}_{\rm G})/\hbar$, of the initial and final Hamiltonian. Using Fermi's golden rule, the direct absorption is calculated as $A_{\rm QD}(\nu) = 2\,{\rm Re}\int_0^\infty dt\, e^{i\nu t}\langle \hat{e}_\uparrow(t)\hat{e}^\dagger_\uparrow\rangle$ and the indirect Mahan absorption as $A_{\rm FR}(\nu) = 2\,{\rm Re}\int_0^\infty dt\, e^{i\nu t}\langle \hat{\Psi}_\uparrow(t)\hat{\Psi}^\dagger_\uparrow\rangle$.[14] Here, we used the notation $\langle \hat{b}_2(t)\hat{b}^\dagger_1\rangle = {\rm Tr}(e^{i\bar{H}^i t}\hat{b}_2 e^{-i\bar{H}^f t}\hat{b}^\dagger_1\varrho)$, where $\hat{b}$ stands for either $\hat{e}_\uparrow$ or $\hat{\Psi}_\uparrow$, $\bar{H}^a = H^a - E^{\rm a}_{\rm G}$, and ϱ is the Boltzmann weight at a FR temperature T.[6] The absorption line shape features a Fano interference, described by the term $A_{\rm I}(\nu) = 2\,{\rm Re}\int_0^\infty dt\, e^{i\nu t}\langle \hat{\Psi}_\uparrow(t)\hat{e}^\dagger_\uparrow\rangle$. The correspondence between the experimental $[A(\Delta E)]$ and theoretical $[A(\nu)]$ spectra follow from $\Delta E = \hbar\nu + \hbar\omega_{\rm th} - \tilde{E}_0$; here, $\tilde{E}_0$ is a fit parameter.[27]

Parameters. The recorded absorption maxima in Fig. 1(b) are fitted with the calculated absorption maxima (black curves) that we obtained from a numerical renormalization group simulation[32] using Eq. (5). A simultaneous fit of the charging plateaus and the X^0 line shapes allows us to extract all experimental parameters.[27] The intradot electron repulsion $U_{\rm ee} = 6.8$ meV is determined by the X^- plateau length. From the $X^0 - X^-$ energy separation, we extract $U_{\rm eh} - U_{\rm ee} = 6.6$ meV, neglecting correlation effects. In the center of the X^0 plateau [Fig. 1(d)], the linewidth is determined by the FR-assisted relaxation into the dark exciton state, which in turn is determined by the gate voltage, the tunneling rate $\Gamma = 400\ \mu$eV,[5] and the dark-bright splitting $\Delta_E = 175\ \mu$eV. The FR is characterized by its bandwidth $W = 2$ meV and its temperature $T = 120$ mK. The best agreement between theory and experiment is obtained for $G_{\rm eh} = 3$ meV and $G_{\rm ee} = 0.7 G_{\rm eh}$. For comparison, we also plot the best fit of the X^0 plateau, if Coulomb scattering is ignored, i.e., $H^a_S \equiv 0$ [Fig. 1(b), gray line]. As a result of the scattering potentials the lengths of the charging plateaus of X^- and X^0 show different extents in gate voltage [Fig. 1(b)]: This is in stark contrast to earlier experiments, which could be explained by assuming exclusively capacitive charging.[27] The renormalized energy of the final bright level with respect to the Fermi energy can be parametrized as $\tilde{\varepsilon}^f_\uparrow(V_g) = \varepsilon_0(V_g) - U_{\rm eh} + \delta\varepsilon_0(V_g)$, where $\delta\varepsilon_0(V_g)$ accounts for a tunneling- and scattering-induced shift of the final bright level. Fitting model predictions to experimental data yields a lever arm of $l = 0.058$, $\varepsilon_0(0.52\ {\rm V}) = 9.205$ meV and $\tilde{\varepsilon}^f_\uparrow(0.52\ {\rm V}) = -4.675$ meV at $V_g = 0.52$ V.

Line shapes. The green curves in Figs. 1(d)–1(i) represent calculated absorption line shapes for the Hamiltonian [Eq. (1)] including the optical interference effect induced by the sample structure.[27] We highlight that we can only reproduce the experimental data using a Fano phase of $\phi = \pi$, corresponding to a constructive Fano interference between the direct and indirect transitions. α is determined by the square root of the ratio of the oscillator strengths of the direct and indirect transitions and is assumed to be independent of the exciton transition energy. In the present experiment we obtain the best agreement between experiment and theory for $\alpha = 0.85$.[27] Figure 1(c) compares the measured maximum absorption amplitudes (dots) versus the calculated absorption amplitudes without adjusting any parameters. The agreement, up to a sample specific proportionality constant and fluctuations of peak contrast of the order of 10% due to alignment, underlines that our model reliably predicts the gate-voltage dependence of the peak absorption. The individual absorption line shapes of the direct (dashed curve), indirect (dotted curve), and interference (dash-dotted curve) terms are exemplarily shown in Fig. 1(i). If the final neutral exciton levels are well below the Fermi energy [Fig. 1(d)], the final state of the optical transition is the dark exciton state, which leads to a homogeneous broadening of the absorption line shape. In the tunneling regime, however, the final state is a correlated many-body state, which is a superposition of the FR states and the QD bright and dark exciton states. Close to the Fermi energy [Fig. 1(i)], the final state has vanishing probability amplitude for finding the electron in the QD. In this regime the QD electron tunnels out into the FR lowering QD hole screening and thereby increasing the effective scattering potential. As a consequence, a screening cloud is formed in the FR that leads to a FES singularity. We emphasize that the absorption strength of the indirect element featuring the FES is very small $(1-\alpha = 0.15)$ and can only be detected due to a significant enhancement by the Fano interference. Due to the spectral overlap of $A_{\rm FR}(\nu)$ and $A_{\rm QD}(\nu)$, we cannot determine experimentally the power-law tail of the FES. However, the good agreement between our experimental data and theory indirectly demonstrates the presence of a FES.

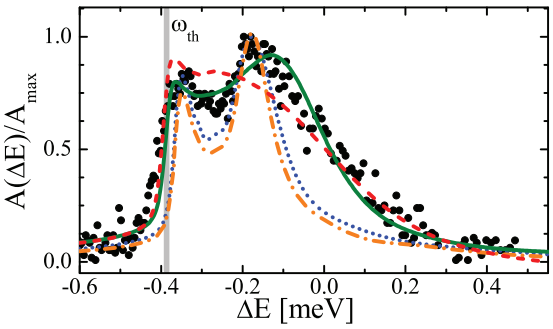

FIG. 3. (Color online) Comparison of the experimental absorption line shape at $V_g = 0.482$ V with theory assuming different scattering scenarios. For the scales, the same conventions were used as for Figs. 1(d)–1(i). The red dashed line shows the best fit for the EAM model ($H^a_S = 0$). Neglecting the electron-electron repulsion ($H^a_S \neq 0$ with $G_{ee} = 0$) the best fit yields the blue dotted curve, while the mean-field approach ($H^a_{\langle S\rangle}$) is shown by the orange dash-dotted curve. The green solid line depicts a dynamic scattering potential.

Dynamical screening. In order to verify the role of the dynamical screening potential, we compare in Fig. 3 our experimental data with theory, for four different screening potentials. (i) The EAM model (dashed line, $H^a_S = 0$) resembles the experimental data for $\nu \gg \Gamma$, indicating the absence of a scattering potential for very short time scales. As the indirect absorption spectrum $A_{FR}(\nu)$ only probes the constant density of states in the FR, the EAM model fails to reproduce the double-peak structure dominating the low-energy part of the spectrum. (ii) Inclusion of a scattering potential leads to the pronounced low-energy peak associated with the FES. Usually, the FES singularity is described by the Mahan–Nozieres–De Dominicis Hamiltonian,[7–9] which considers a scattering potential G_{eh} while neglecting any Coulomb repulsion between QD and FR electrons, i.e., $G_{ee} = 0$ (dotted curve). (iii) A possible way to include the latter interaction in our description while still using, for simplicity, a time-independent scattering potential would be to use a mean QD electron occupation, $H^a_{\langle S\rangle} = (G_{ee}\sum_\sigma \langle \hat{n}_\sigma(t \to \infty)\rangle - G_{eh}\delta_{x,f})\sum_{\sigma'}(\hat{\Psi}^\dagger_{\sigma'}\hat{\Psi}_{\sigma'} - \frac{1}{2})$ (dash-dotted line). The models (ii) and (iii) both feature a second peak in the absorption spectrum in the long-time limit ($\nu \ll \Gamma$), but the absorption line shapes strongly deviate from the experimental data for short-time scales ($\nu \gg \Gamma$). (iv) Using the dynamical screening model of Eq. (4), we allow the QD electron occupation and thereby the screening of the QD hole potential to evolve in time. As depicted by the solid line, this dynamical screening model yields good agreement with experiment for all energy scales, showing that a scattering potential, and consequently an electron screening cloud in the FR, forms on time scales on the order of reciprocal Γ.

In contrast to prior nonresonant excitation experiments,[26] we directly observe a correlated many-body state formed by the direct and indirect exciton transitions and develop a model to quantify the potential scattering strength. We note that our model assumes a perfect screening potential.[15] A partial screening of the scattering potential due to imperfections in the FR would lead to a stronger power-law decay of the FES,[20,33,34] which could explain the residual difference between experiment and theory. In conclusion, we demonstrated a *dynamic* regime of Fermi-edge physics that highlights the importance of optically active quantum dots in the investigation of quantum impurity physics.

We acknowledge helpful discussions with B. Sbierski. This work was supported by an ERC Advanced Investigator Grant (F.H., S.S., W.W., J-M.S., A.I.). J.v.D., M.H., and A.W. acknowledge DFG via NIM, SFB631, SFB-TR12, and WE4819/1-1.

*fhaupt@phys.ethz.ch; http://www.quantumphotonics.ethz.ch

[1] P. W. Anderson, Phys. Rev. Lett. **18**, 1049 (1967).
[2] A. K. Geim, P. C. Main, N. LaScala, L. Eaves, T. J. Foster, P. H. Beton, J. W. Sakai, F. W. Sheard, M. Henini, G. Hill, and M. A. Pate, Phys. Rev. Lett. **72**, 2061 (1994).
[3] H. Frahm, C. von Zobeltitz, N. Maire, and R. J. Haug, Phys. Rev. B **74**, 035329 (2006).
[4] E. E. Vdovin, Y. N. Khanin, O. Makarovsky, Y. V. Dubrovskii, A. Patane, L. Eaves, M. Henini, C. J. Mellor, K. A. Benedict, and R. Airey, Phys. Rev. B **75**, 115315 (2007).
[5] C. Latta, F. Haupt, M. Hanl, A. Weichselbaum, M. Claassen, W. Wuester, P. Fallahi, S. Faelt, L. Glazman, J. von Delft, H. E. Tureci, and A. Imamoglu, Nature (London) **474**, 627 (2011).
[6] H. E. Tureci, M. Hanl, M. Claassen, A. Weichselbaum, T. Hecht, B. Braunecker, A. Govorov, L. Glazman, A. Imamoglu, and J. von Delft, Phys. Rev. Lett. **106**, 107402 (2011).
[7] G. D. Mahan, Phys. Rev. **163**, 612 (1967).
[8] P. Nozieres and C. de Domini, Phys. Rev. **178**, 1097 (1969).
[9] L.N. Oliveira and J.W. Wilkins, Phys. Rev. B **32**, 696 (1985).
[10] K. Ohtaka and Y. Tanabe, Rev. Mod. Phys. **62**, 929 (1990).
[11] H. Neddermeyer, Phys. Rev. B **13**, 2411 (1976).
[12] T. Ishii, T. Shii, Y. Sakisaka, S. Yanaguchi, T. Hanyu, and H. Ishii, J. Phys. Soc. Jpn. **42**, 876 (1977).
[13] T. A. Callcott, E. T. Arakawa, and D. L. Ederer, Phys. Rev. B **18**, 6622 (1978).
[14] G. D. Mahan, Phys. Rev. **153**, 882 (1967).
[15] P. Hawrylak, Phys. Rev. B **44**, 3821 (1991).
[16] C. L. Kane, K. A. Matveev, and L. I. Glazman, Phys. Rev. B **49**, 2253 (1994).
[17] U. Fano, Phys. Rev. **124**, 1866 (1961).
[18] M. S. Skolnick, J. M. Rorison, K. J. Nash, D. J. Mowbray, P. R. Tapster, S. J. Bass, and A. D. Pitt, Phys. Rev. Lett. **58**, 2130 (1987).
[19] W. Chen, M. Fritze, A. V. Nurmikko, D. Ackley, C. Colvard, and H. Lee, Phys. Rev. Lett. **64**, 2434 (1990).
[20] G. Yusa, H. Shtrikman, and I. Bar-Joseph, Phys. Rev. B **62**, 15390 (2000).
[21] V. Huard, R. T. Cox, K. Saminadayar, A. Arnoult, and S. Tatarenko, Phys. Rev. Lett. **84**, 187 (2000).
[22] J. M. Calleja, A. R. Goni, B. S. Dennis, J. S. Weiner, A. Pinczuk, S. Schmittrink, L. N. Pfeiffer, K. W. West, J. F. Muller, and A. E. Ruckenstein, Solid State Commun. **79**, 911 (1991).

[23]M. Fritze, A. V. Nurmikko, and P. Hawrylak, Surf. Sci. **305**, 580 (1994).

[24]P. Hawrylak, Phys. Rev. B **44**, 6262 (1991).

[25]M. Heyl and S. Kehrein, Phys. Rev. B **85**, 155413 (2012).

[26]N. A. J. M. Kleemans, J. van Bree, A. O. Govorov, J. G. Keizer, G. J. Hamhuis, R. Notzel, A. Y. Silov, and P. M. Koenraad, Na. Phys. **6**, 534 (2010).

[27]See Supplemental Material at http://link.aps.org/supplemental/10.1103/PhysRevB.88.161304 for details on experimental techniques, sample properties and theoretical model.

[28]R. J. Warburton, C. Schaflein, D. Haft, F. Bickel, A. Lorke, K. Karrai, J. M. Garcia, W. Schoenfeld, and P. M. Petroff, Nature (London) **405**, 926 (2000).

[29]A. Hogele, S. Seidl, M. Kroner, K. Karrai, R. J. Warburton, B. D. Gerardot, and P. M. Petroff, Phys. Rev. Lett. **93**, 217401 (2004).

[30]P. A. Dalgarno, M. Ediger, B. D. Gerardot, J. M. Smith, S. Seidl, M. Kroner, K. Karrai, P. M. Petroff, A. O. Govorov, and R. J. Warburton, Phys. Rev. Lett. **100**, 176801 (2008).

[31]This assumption neglects the anisotropic exchange splitting between the bright states. In our description we fix the hole spin to be $|\Downarrow\rangle$ without loss of generality (Ref. 27).

[32]A. Weichselbaum and J. von Delft, Phys. Rev. Lett. **99**, 076402 (2007); A. Weichselbaum, Phys. Rev. B **86**, 245124 (2012).

[33]Y. Gefen, R. Berkovits, I. V. Lerner, and B. L. Altshuler, Phys. Rev. B **65**, 081106 (2002).

[34]D. A. Abanin and L. S. Levitov, Phys. Rev. Lett. **93**, 126802 (2004).